World Academy of Science, Engineering and Technology
International Journal of Biomedical and Biological Engineering
Vol:11, No:4, 2017

Developing Models for Predicting Physiologically Impaired Arm Reaching Paths

Nina Robson, Kenneth John Faller II, Vishalkumar Ahir, Mustafa Mhawesh, Reza Langari

Abstract**—**This paper describes the development of a model of an impaired human arm performing a reaching motion, which will be used to predict hand path trajectories for people with reduced arm joint mobility. Assuming that the arm was in contact with a surface during the entire movement, the contact conditions at the initial and final task locations were determined and used to generate the entire trajectory. The model was validated by comparing it to experimental data, which simulated an arm joint impairment by physically constraining the joint motion with a brace. Future research will include using the model in the development of physical training protocols that avoid early recruitment of "healthy" Degrees-Of-Freedom (DOF) for reaching motions, thus facilitating an Active Range-Of-Motion Recovery (AROM) for a particular impaired joint.

Keywords**—**Higher order kinematic specifications, human motor coordination, impaired movement, kinematic synthesis.

I. Introduction

THE motor control and learning mechanisms of the Central Nervous System (CNS) enables optimal and robust motor control performance during arm reaching movements. The arm reaching task can be defined as moving the hand from an initial to a final position. In order to achieve the desired hand kinematics, the end-effector trajectory must be planned. However, there are an infinite number of possible satisfactory trajectories. In addition, from the motor control perspective, the trajectory needs to be converted from task coordinates to joint coordinates to specify the control commands for each independent joint motion. However, since the number of independent joint DOF of the human arm is greater than the six DOF used for the manipulation task (i.e., three for position and three for orientation), the trajectory planning using joint coordinates becomes a kinematically redundant mapping problem which, from an actuation perspective, is due to the multiple connections of skeletal muscles used during each joint motion. By adopting Failure Recovery Synthesis (FRS) strategies, the model can perform the optimal motion to achieve the desired task kinematics with minimal energy consumption.

In general, a normal arm reaching movement of a healthy subject is known to follow the geodesic (i.e., the shortest path) with the minimum jerk velocity (i.e., a bell-shaped speed profile for the maximized smoothness of the motion) [1]. Optimal motion planning seems consistent even under physical constraint conditions. In their study regarding arm reaching movements on a constraint force surface, Sha et al. showed that healthy subjects keep trying to follow the geodesic with the minimum jerk velocity [2]. Roby-Brami et al. found that the stroke patients seek a way to recover the original control strategies through therapeutic arm reaching tasks against their physical impairments (e.g., reduced Joint Range Of Motion (JROM), paralysis, and excessive joint stiffness) [3]. The paper was based on the assumption that the consistency of the human motion planning strategy will be kept, even under a joint failure condition.

Nina Robson, Vishalkumar Ahir and Mustafa Mhawesh are with the Mechanical Engineering Department, California State University, Fullerton (e-mail: nrobson@fullerton.edu)

Kenneth John Faller is with the Computer Engineering Program, California State University, Fullerton (e-mail: jfaller@fullerton.edu).

Reza Langari is with the Mechanical Engineering Department, Texas A&M University (e-mail: rlangari@tamu.edu).

II. Models for Predicting Impaired Reaching Movements

The impaired hand model should match the subject's anthropometric arm data, thus the kinematic skeleton of the arm of the patient needs to be calculated. The kinematic skeleton was defined as the set of joint axis locations and orientations that recreate the motion of the hand in space. A robotics approach was used to approximate the skeleton (i.e., rigid bodies connected by revolute joints). Using this model, the motion of the arm can be expressed in a straightforward way, using a predetermined number of joint angles for each pose. There exist several methods to obtain the description of the robotic arm skeleton. Many of the studies done so far present joint axes associated with an anatomic joint. However, due to the variability in the skeleton dimensions, it needs to be calculated or modified for each individual to obtain the desired accuracy [1]. Existing approaches are precise, however, require the use of expensive equipment (e.g., x-rays (mainly for cadavers or MRI) and are very time-consuming [2]. As a result, these techniques are a solid standard for comparison to verify experimental results but cannot be incorporated in systems used by many subjects. A solution more suited for this can be achieved by combining anatomic measurements with a motion-based kinematic synthesis (Fig. 1) [3]-[5]. This solution consists of five major steps:

1. A non-dimensional kinematic model of an impaired arm, with reduced mobility in a particular joint, was developed and incorporated anatomical human arm data.
2. A kinematic task that consists of higher order kinematic constraints, compatible with contact and curvature constraints, was specified.
3. The kinematic synthesis equations, specific to the kinematic chain, were solved to obtain the locations of the fixed (shoulder) and the moving (wrist) pivots.

4. The determined locations from Step 3, which define the kinematic skeleton for a specific subject within a margin of error, was then be used to reconstruct the skeleton.
5. Trajectory planning.

The skeleton must be capable of performing a realistic motion based entirely on the set of joint angles provided by the synthesis/analysis algorithm described above.

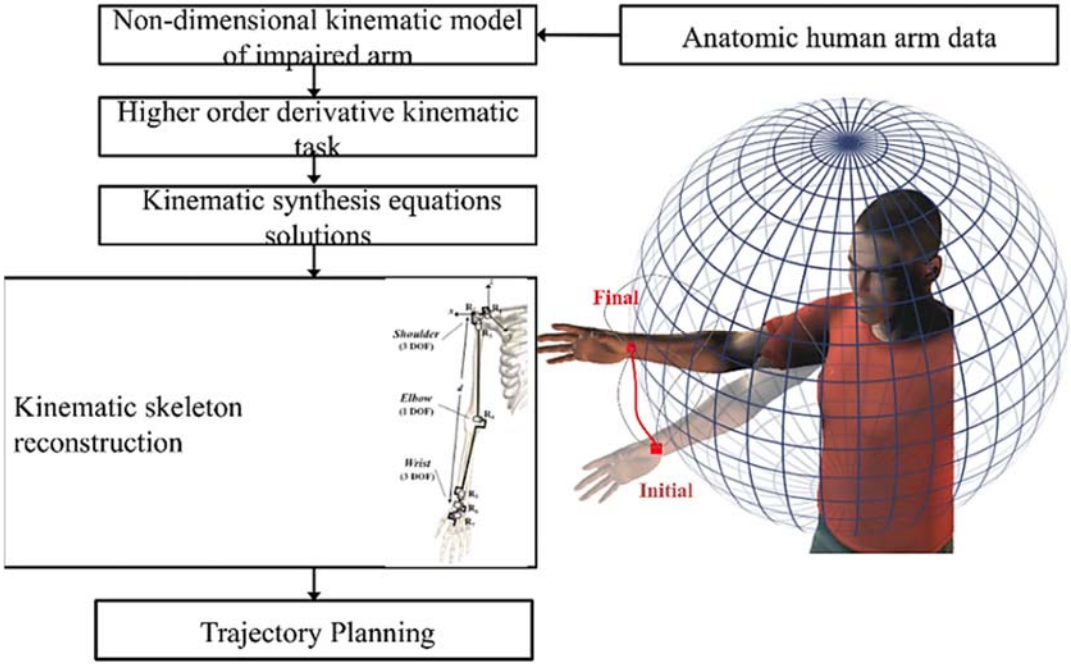

Fig. 1 Kinematic skeleton extraction

III. Kinematic Models of Joint Impaired Arm

In this section, it is described how portions of the FRS method for robot manipulators mounted on a movable platform [6]-[8], based on kinematic synthesis techniques, were used. The FRS locks in place the failed arm joint and derives position, velocity, and acceleration constraint equations according to the geometrical constraints due to the failure and contact with objects in the environment. The design equations can be solved numerically using the Polynomial Homotopy Continuation (PHC) pack software [9] to determine a new position for the arm base/movable platform and a new grasping location for the end-effector. The recovery strategy can be applied to any platform-robot system, in which free parameters exist, that allows the reconfiguration of the system to adapt to a joint failure. From the reconfigured manipulator locations, entire trajectories of the robotic joint DOF were planned through modifications of the robotic trajectory planning techniques introduced in [10].

In what follows, portions from the strategy for recovery planning for a general three DOF arm, with a three DOF spherical wrist, were used. It was assumed the arm has the general six DOF structure of a PUMA-like robot which we term a TRS* arm [11]. Hence, the six DOF consist of rotary actuators that control the shoulder azimuth, shoulder elevation, elbow, and spherical wrist. It was assumed that there was a joint failure in each one of the arm actuators (except in the wrist), modeling the crippled chain as parallel RRS, perpendicular RRS, and TS chain, respectively. TS and RRS position synthesis has been solved in McCarthy [12] and Hai-Jun Su *et al.* [13]. It happens that the solution technique remains valid if one specifies positions and velocities rather than just task positions. However, if one specifies acceleration, the synthesis becomes complicated and has been recently solved by Robson *et al.* [7], [8].

A. Human Joint Impairment as a Kinematic Synthesis Problem

Shown in Fig. 2 is a six DOF TRS arm in which the first two revolute joints intersect and are perpendicular to each other and the last three revolute joints intersect at a point to define a spherical wrist. The goal here was to model the system to obtain each of the five DOF chains resulting from failures of joints S_1, S_2, and S_3, respectively.

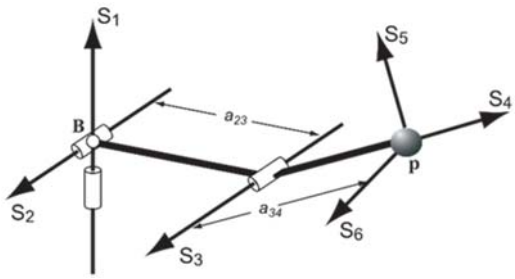

Fig. 2 Kinematic structure of a general six DOF TRS chain, which represents a simplified model of a human arm

* T refers to two revolute joints that intersect at right angles, also called Hooke's joint, R is a revolute or hinged joint, and S is a spherical wrist.

B. Arm Failure Models

1. Joint S_1 Failure "Parallel RRS Chain"

Joint S_1 provides the azimuth rotation of the shoulder of the arm (see Fig. 2), and its failure reduces the TRS serial chain to a five DOF RRS chain in which the first two R-joints were parallel, hence a "parallel RRS" chain, as shown in Fig. 3. This chain had the property that the trajectory P(t) of the wrist center lies on a plane through B and normal to the direction **B** = (B_x, B_y, B_z). Details on the constraint equations and their solution can be found in [7], [8].

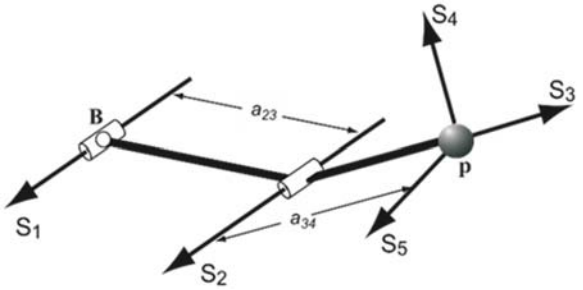

Fig. 3 The parallel RRS chain, which represents a simplified kinematic structure of a human arm with a reduced shoulder azimuth joint mobility

2. Joint S_2 Failure "Perpendicular RRS Chain"

Joint S_2 provides the elevation rotation at the shoulder of the arm (see Fig. 2), and its failure reduces the TRS serial chain to a five DOF RRS chain, in which the first two R-joints were perpendicular (i.e., a "perpendicular RRS" arm) shown in Fig. 4. This chain had the property that the trajectory of the wrist center P lies on a right circular torus generated by a circle around the axis S_3 that was then swept around the joint axis S_1 [13]. In general, the synthesis of an *RRS* with an elevation actuator failure requires solving for 10 free parameters, two for S_1, three for P, three for B, and the two link lengths $R = a34$ and ρ (if not specified) to achieve a defined task despite the S_2 joint failure. Details on the constraint equations and their solution can be found in [7], [8].

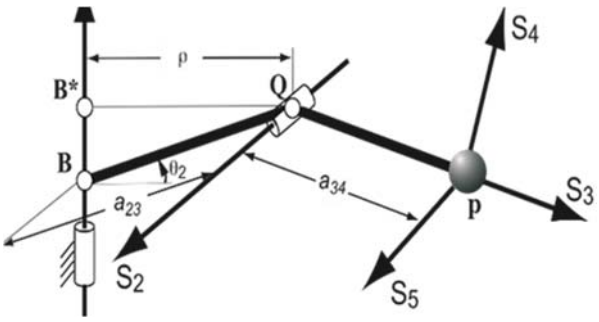

Fig. 4 The perpendicular RRS chain, which represents a simplified kinematic structure of a human arm with a reduced mobility in the shoulder elevation joint rotation

3. Joint S_3 Failure "TS Chain"

Joint S_3 was the elbow joint of the arm (see Fig. 2), and its failure, which resulted in a five DOF TS serial chain, shown in Fig. 5. A five DOF TS chain can position the wrist center P on a sphere with radius R about the base point **B**. Details on the constraint equations and their solution can be found in [7], [8].

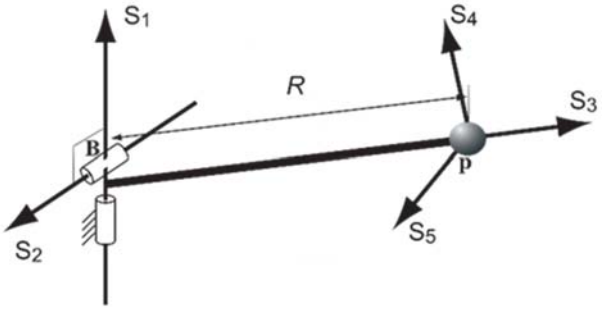

Fig. 5 The TS chain, which represents the simplified kinematic structure of a human arm with a reduced mobility in the elbow joint $\mathbf{S_3}$

After the non-dimensional kinematic models of the impaired arms were defined, the kinematic task was specified. It consisted of positions and higher order kinematic constraints, compatible with contact and curvature specifications between the arm and the objects/environment. The incorporation of anatomic human arm data within the crippled models allowed for the solution to the kinematic synthesis equations for the given task. The solutions resulted in a kinematic skeleton reconstruction. In the following section, the elbow joint failure case was studied and a model for predicting the elbow-impaired reaching path was developed and validated.

IV. Kinematics of an Elbow Constrained Arm

Fig. 6 shows the schematic diagram of the concept of the proposed method. The kinematic configuration of an anthropomorphic robotic manipulator with seven DOF was considered. The Spherical-Revolute-Spherical (SRS) robotic arm with an elbow failure resulted in a six DOF Spherical-Spherical (SS) kinematic chain with a constant length R†. When the elbow joint was fixed at a certain angle, the kinematic structure of the arm changed to a serial SS chain, characterized by a spherical workspace centered at the shoulder. In order to represent motion kinematics of the elbow constrained arm, Extrinsic Task Coordinates (ETC) shown in Fig. 7 were defined [14]. In the figure, a virtual link connecting the shoulder and the wrist position was drawn as a thick solid line and guidelines for representing the spherical workspace were drawn as thin lines. The coordinate system consists of latitude, longitude, and swivel angle of the virtual link, and roll, pitch, and yaw of the wrist joint. This was further simplified by considering the three wrist DOFs, related to the hand orientation, as fixed. This was done because of their lack of influence on the positioning of the end-effector.

† Note that due to the roll angles in both shoulder and wrist joints, the arm DOF can be further reduced to a TS chain.

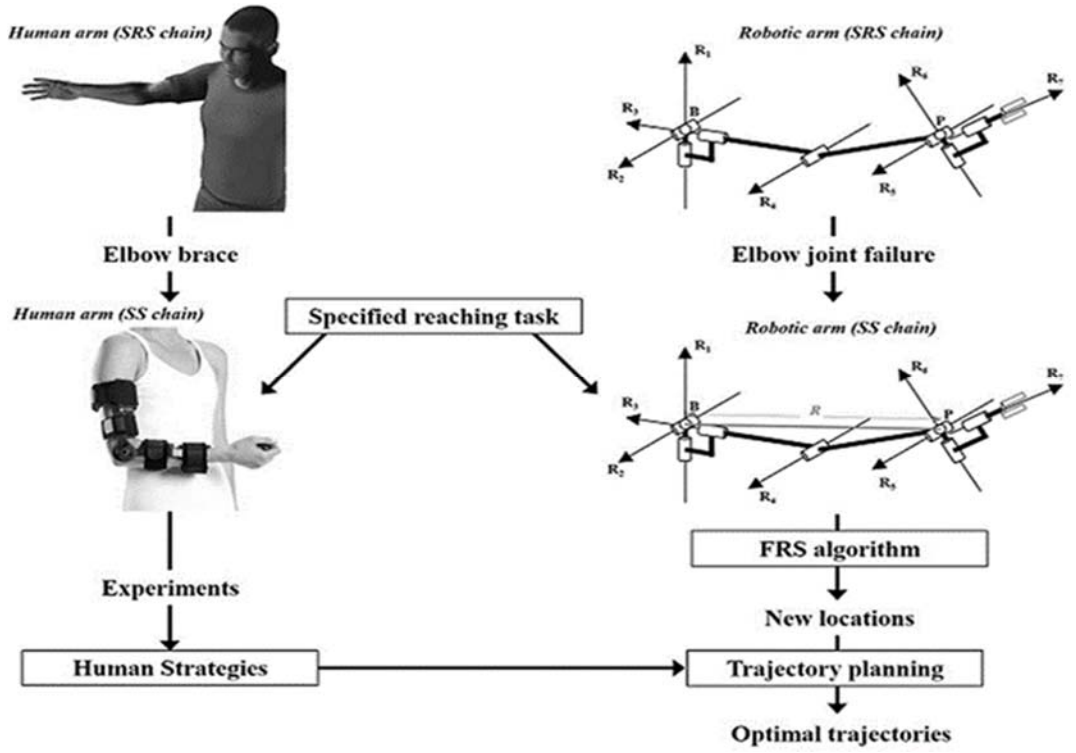

Fig. 6 Conceptual diagram of the trajectory planning model, which integrates knowledge from FRS, as well as experimental observations on elbow constrained reaching movements

The end-effector (or the hand) location $(\mathrm{x_h}, \Theta_h)^{\mathrm{T}} = (x_h, y_h, z_h, \phi, \theta, \psi)^{\mathrm{T}}$ in the fixed frame F was obtained by the forward kinematics:

$$\begin{bmatrix} x_h \\ y_h \\ z_h \\ \phi \\ \theta \\ \psi \end{bmatrix} = \begin{bmatrix} d\cos\alpha \sin\beta \\ d\cos\alpha \cos\beta \\ d\sin\alpha \\ \arctan 2(R_{23}, R_{33}) \\ \arcsin(R_{13}) \\ \arctan 2(R_{12}, R_{11}) \end{bmatrix} \quad (1)$$

where d is a constant for the distance between the shoulder S joint and the wrist S joint and R_{ij} is the (i, j) component of the rotation matrix R from the fixed frame F to the moving frame M that was obtained from:

$$\begin{aligned} R_{11} &= s_\varsigma(s_\epsilon(c_\beta c_\gamma s_\delta - c_\beta s_\gamma c_\delta) + c_\epsilon s_\beta) + c_\varsigma(c_\beta c_\gamma c_\delta + c_\beta s_\gamma s_\delta), \\ R_{12} &= -s_\varsigma(c_\beta c_\gamma c_\delta + c_\beta s_\gamma s_\delta) + c_\varsigma(s_\epsilon(c_\beta c_\gamma s_\delta - c_\beta s_\gamma c_\delta) + s_\beta c_\epsilon), \\ R_{13} &= -s_\epsilon s_\beta + c_\epsilon(c_\beta c_\gamma s_\delta - c_\beta s_\gamma c_\delta), \\ R_{23} &= s_\epsilon(c_\alpha c_\beta - s_\alpha c_\gamma) + c_\epsilon(s_\delta(s_\alpha s_\gamma + c_\alpha s_\beta c_\gamma) - c_\alpha s_\beta s_\gamma c_\delta), \\ R_{33} &= -s_\epsilon(s_\alpha c_\beta + c_\alpha c_\gamma) + c_\epsilon(s_\delta(c_\alpha s_\gamma - s_\alpha s_\beta c_\gamma) + s_\alpha s_\beta s_\gamma c_\delta), \end{aligned} \quad (2)$$

where sin(.) and cos(.) are denoted as s(.) and c(.). From the geometry of the manipulator configuration, each joint angle was derived by the inverse kinematics as:

$$\begin{bmatrix} \alpha \\ \beta \\ \gamma \\ \delta \\ \epsilon \\ \varsigma \end{bmatrix} = \begin{bmatrix} \arcsin(z_h/d) \\ \arctan 2(x_h, y_h) \\ \mathrm{sign}\left((\mathrm{n_{ap}} \times \mathrm{n_v}) \cdot \mathrm{x_h}\right) \arccos(\mathrm{n_v} \cdot \mathrm{n_{ap}}) \\ \arctan 2(s_\theta, c_\phi c_\theta) \\ -\arcsin(-s_\phi c_\theta) \\ \arctan 2(c_\phi s_\psi + s_\phi s_\theta c_\psi, c_\phi c_\psi - s_\phi s_\theta s_\psi) \end{bmatrix} \quad (3)$$

where the swivel angle ψ is defined as the angle between the manipulator arm plane and the vertical plane [15]. In (3), $\mathrm{n_v}$ and $\mathrm{n_{ap}}$ refer to the unit normal vectors to the vertical plane and the arm plane, respectively, which are defined as:

$$\mathrm{n_v} = \frac{\mathrm{u_{-z}} \times \mathrm{x_h}}{||\mathrm{u_{-z}} \times \mathrm{x_h}||} \quad \text{and} \quad \mathrm{n_{ap}} = \frac{\mathrm{x_e} \times \mathrm{x_h}}{||\mathrm{x_e} \times \mathrm{x_h}||} \quad (4)$$

where $\mathrm{u_{-z}}$ represents the unit vector for the negative z-axis of the fixed frame F, and $\mathrm{x_e} = [\mathrm{x_e}, \mathrm{y_e}, \mathrm{z_e})^{\mathrm{T}}$ and $\mathrm{x_h} = [\mathrm{x_h}, \mathrm{y_h}, \mathrm{z_h}]^{\mathrm{T}} \mathrm{x_e} = [\mathrm{x_e}, \mathrm{y_e}, \mathrm{z_e}]^{\mathrm{T}}$ and $\mathrm{x_h} = [\mathrm{x_h}, \mathrm{y_h}, \mathrm{z_h}]^{\mathrm{T}}$ indicate position vectors of the manipulator's elbow and the wrist in F.

V. Higher Order Motion Task Specifications Defined From Relative Curvatures of Contact

In the following section, the process for extracting the desired end-effector (or hand) kinematics of an elbow constrained human arm at the selected task locations (i.e., the initial and the final end-effector locations in a reaching task) is described.

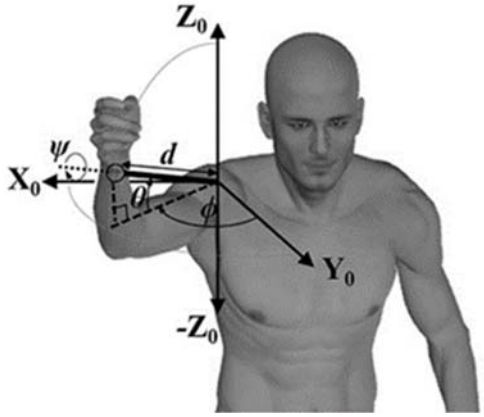

Fig. 7 The defined ETC that represents an elbow constrained anthropomorphic manipulator kinematics [14]

Fig. 3 presents a schematic plot of an elbow constrained anthropomorphic manipulator, as well as the geometry of the spatial contact of its end-effector in the vicinity of a particular task location [16]. It can be assumed that the hand was in contact with objects or the environment at three points A, B, and C. The object/environment geometry in the vicinity of the contact was represented by three spheres with radii of curvature R_A, R_B and R_C, respectively. The orientation angles $\phi(t)$, $\theta(t)$ and $\psi(t)$ of the moving frame M were directly derived from the end-effector contact positions as presented in [17]:

$$\phi(t) = \arctan 2\left(\frac{\hat{k}\cdot\big((\mathrm{B}-\mathrm{A})\times(\mathrm{C}-\mathrm{A})\big)\times(\mathrm{B}-\mathrm{A})}{\big|\big((\mathrm{B}-\mathrm{A})\times(\mathrm{C}-\mathrm{A})\big)\times(\mathrm{B}-\mathrm{A})\big|}, \frac{\hat{k}\cdot((\mathrm{B}-\mathrm{A})\times(\mathrm{C}-\mathrm{A}))}{|(\mathrm{B}-\mathrm{A})\times(\mathrm{C}-\mathrm{A}))|}\right),$$
$$\theta(t) = -\arcsin\frac{\hat{k}\cdot(\mathrm{B}-\mathrm{A})}{|\mathrm{B}-\mathrm{A}|},$$
$$\psi(t) = -\arctan 2\left(\frac{\hat{\jmath}\cdot(\mathrm{B}-\mathrm{A})}{|\mathrm{B}-\mathrm{A}|}, \frac{\hat{\imath}\cdot(\mathrm{B}-\mathrm{A})}{|\mathrm{B}-\mathrm{A}|}\right), \quad (5)$$

where $\hat{\imath}$, $\hat{\jmath}$ and $\hat{k}$ are unit vectors along each axis of the fixed frame F. The directions of the velocity vectors A, B, and C were constrained to be perpendicular to the direction of the radii of the contact spheres [17]:

$$\begin{aligned}\dot{\mathrm{A}} &= \mathrm{w}\times(\mathrm{A}-\mathrm{d}) + \dot{\mathrm{d}} = \mathrm{w}_{\mathrm{O_1A}}\times(\mathrm{A}-\mathrm{O_1})\\ \dot{\mathrm{B}} &= \mathrm{w}\times(\mathrm{B}-\mathrm{d}) + \dot{\mathrm{d}} = \mathrm{w}_{\mathrm{O_2B}}\times(\mathrm{B}-\mathrm{O_2})\\ \dot{\mathrm{C}} &= \mathrm{w}\times(\mathrm{C}-\mathrm{d}) + \dot{\mathrm{d}} = \mathrm{w}_{\mathrm{O_3C}}\times(\mathrm{C}-\mathrm{O_3})\end{aligned} \quad (6)$$

where $\mathrm{w} = R_0(R_1)^{-1}$ is a function of $\dot{\phi}$, $\dot{\theta}$, and $\dot{\psi}$ that defines the screw axis of M. Here, R_0 and R_1 refer the rotation matrix of M and its first order time derivative both at $t = 0$. The vector d represents the translation displacement of the moving frame M within F (i.e., d = A). By solving (6) for **w**, the angular velocities $\dot{\phi}$, $\dot{\theta}$, and $\dot{\psi}$ were derived.

In the same manner, the contact points A, B, and C were guided along trajectories with radii of curvature R_A, R_B and R_C, since the moving frame M moves in contact with three spheres. By differentiating (6), the equations for acceleration task specifications were derived as:

$$\begin{aligned}\ddot{\mathrm{A}} &= \mathrm{a}_{\mathrm{O_1A}}\times(\mathrm{A}-\mathrm{O_1}) + \mathrm{w}_{\mathrm{O_1A}}\times(\mathrm{w}_{\mathrm{O_1A}}\times(\mathrm{A}-\mathrm{O_1}))\\ &= \mathrm{a}\times(\mathrm{A}-\mathrm{d}) + \mathrm{w}\times\big(\mathrm{w}\times(\mathrm{A}-\mathrm{d})\big) + \ddot{\mathrm{d}},\\ \ddot{\mathrm{B}} &= \mathrm{a}_{\mathrm{O_2B}}\times(\mathrm{B}-\mathrm{O_2}) + \mathrm{w}_{\mathrm{O_2B}}\times(\mathrm{w}_{\mathrm{O_2B}}\times(\mathrm{B}-\mathrm{O_2}))\\ &= \mathrm{a}\times(\mathrm{B}-\mathrm{d}) + \mathrm{w}\times\big(\mathrm{w}\times(\mathrm{B}-\mathrm{d})\big) + \ddot{\mathrm{d}},\\ \ddot{\mathrm{C}} &= \mathrm{a}_{\mathrm{O_3C}}\times(\mathrm{C}-\mathrm{O_3}) + \mathrm{w}_{\mathrm{O_3C}}\times(\mathrm{w}_{\mathrm{O_3C}}\times(\mathrm{C}-\mathrm{O_3}))\\ &= \mathrm{a}\times(\mathrm{C}-\mathrm{d}) + \mathrm{w}\times\big(\mathrm{w}\times(\mathrm{C}-\mathrm{d})\big) + \ddot{\mathrm{d}},\end{aligned} \quad (7)$$

where a is the derivative of **w** and is a function of $\ddot{\phi}$, $\ddot{\theta}$ and $\ddot{\psi}$ after substituting the values ϕ, θ, ψ, $\dot{\phi}$, $\dot{\theta}$ and $\dot{\psi}$ [17].

This resulted in position, velocity, and acceleration task specifications, compatible with contact and curvature constraints between the arm and objects/environment. They were directly used in the synthesis equations and trajectory planning generation, which is the subject of the following sections.

VI. The TS Model Synthesis Equations

Recall that a TS chain is formed when a body is connected to the ground by a gimbal joint and to a floating link by a spherical joint (see Fig. 5). The movement of the floating link used was connected by the TS chain such that the trajectory of **P** in F lies on a sphere, with a radius R, about **B.** The TS chain had seven design parameters, the coordinates of the center of the intersection of the perpendicular revolute joints (R-joints) in the base frame, the coordinates of the intersection of the last three R-joints in the moving frame, and the length R of the distance between these points. The synthesis procedure computed these parameters $\mathbf{r} = (B_x, B_y, B_z, P_x, P_y, P_z, R)$ by solving seven constraint equations that must be met for the chain to achieve a prescribed task.

A formulation of the constraint equations for the TS chain was derived, by considering the position, velocity, and acceleration constraints imposed on a point in a moving body [7], [8], [18]. The trajectory $\mathbf{P}(t)$ of the center of the S-joint, connected to the floating link, was positioned on a sphere about the center **B** of the fixed T-joint that was:

$$(\mathrm{P}(t) - \mathrm{B}) \cdot (\mathrm{P}(t) - \mathrm{B}) = R^2 \quad (8)$$

where R is the length of the TS chain. The derivatives of this equation provided the velocity constraint equation:

$$\frac{d}{dt}\mathbf{P} \cdot (\mathbf{P} - \mathbf{B}) = 0 \quad (9)$$

and the acceleration constraint equation:

$$\frac{d^2}{dt^2}\mathbf{P}\cdot(\mathbf{P}-\mathbf{B})+(\frac{d}{dt}\mathbf{P})\cdot(\frac{d}{dt}\mathbf{P})=0 \quad (10)$$

In order to determine the seven design parameters, seven design equations were required. Choosing one of the task positions to be first and using the relative displacement matrices $D_{1j} = [K_0^j][K_0^1]^{-1}$ allowed for the definition of coordinates $\mathbf{P}^j$ taken by the moving pivot as:

$$\mathbf{P}^j = [D_{1j}][\mathbf{P}^1] \quad (11)$$

Thus, for each of the n task positions, the position, velocity, and acceleration design equations were:

$$\begin{aligned} P_j &: ([D_{1j}]\mathbf{P}^1-\mathbf{B})\cdot([D_{1j}]\mathbf{P}^1-\mathbf{B}) = R^2,\\ V_j &: ([\Omega^j][D_{1j}]\mathbf{P}^1)\cdot([D_{1j}]\mathbf{P}^1-\mathbf{B}) = 0,\\ A_j &: ([\Lambda^j][D_{1j}]\mathbf{P}^1)\cdot([D_{1j}]\mathbf{P}^1-\mathbf{B}) + ([\Omega^j][D_{1j}]\mathbf{P}^1)\cdot\\ &\quad ([\Omega^j][D_{1j}]\mathbf{P}^1) = 0, j = 1,\ldots,n. \end{aligned} \quad (12)$$

Note that for the case of constraint/lower mobility elbow joint, the variable R or the range of R was known. Thus, in general, six equations were needed to solve for the unknown parameters $\mathbf{r} = (B_x, B_y, B_z, P_x, P_y, P_z)$. The polynomial system formed by (12) consists of five quadratic equations and has a total degree of $2^5 = 32$. An algebraic solution to this problem based on elimination methods has been proposed [7], [8]. The solution procedure required 25 seconds to compute the results on a Dual 1.8 GHz PowerPC G5.

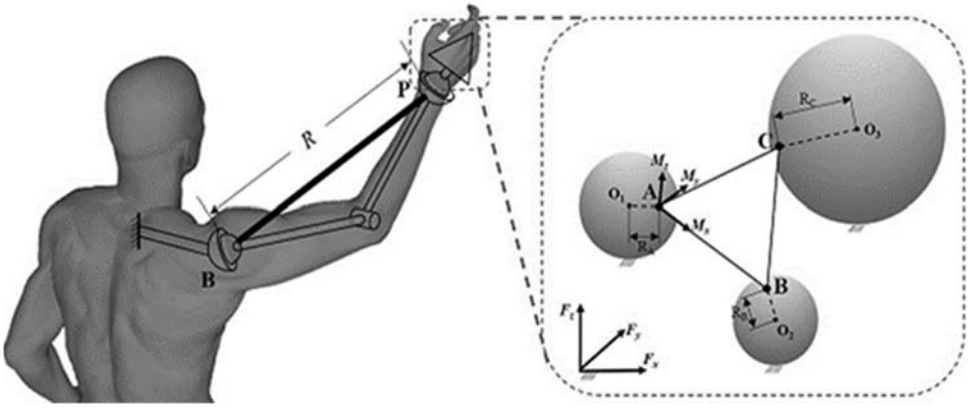

Fig. 8 Schematic plot of an elbow constrained arm with contact specifications. B and P refer to positions of the base and the moving pivot, respectively [16]

VII. Trajectory Generation Method

From previous experimental observations on the elbow constrained human arms performing a reaching movement, it can be inferred that the human CNS generates the hand motion in the constrained task coordinates (i.e., spherical coordinates centered at the shoulder joint for the elbow constrained arm workspace) rather than the anatomical joint coordinates [14], [19], [20]. Therefore, the arm kinematics were defined in ETC. In addition, defining in ETC enables the separation of the trajectory planning of the redundant DOF (i.e., the swivel angle γ) from the end-effector motion planning. Note that the end-effector position x_h was not dependent on the swivel angle γ (see (1)). In order to generate the entire end-effector trajectory connecting two task locations, modification of the trajectory planning techniques, incorporating higher order motion constraints introduced in [10], was adopted.

At each task point, the inverse kinematics of the elbow constrained manipulator, shown in (3), enables the conversion of a specified manipulator configuration into joint angles. The joint angular velocity vector $\dot{q}_i = (\dot{\alpha}_i, \dot{\beta}_i, \dot{\gamma}_i, \dot{\delta}_i, \dot{\epsilon}_i, \dot{\varsigma}_i)^T$ at the i-th task point was solved by:

$$V_i = J_i\dot{q}_i, \quad (13)$$

where $V_i = (v_i^T, w_i^T)$ is the linear and angular velocity specifications of the moving frame M in the fixed frame F and J_i refers to the Jacobian of the forward kinematics (see (1)) at the i-th task point. When some of the DOFs of the manipulator (e.g., excluding wrist DOF for its minor role in the positioning task as assumed in [16]) were excluded, the Jacobian J_i was not a square matrix. In this case, a pseudo-inverse was utilized to solve (13). The prescribed linear and angular accelerations of the moving frame M in the fixed frame F, $A_i = (a_i^T, \alpha_i^T)$, can be mapped to a corresponding joint angular acceleration vector $\ddot{q}_i = (\ddot{\alpha}_i, \ddot{\beta}_i, \ddot{\gamma}_i, \ddot{\delta}_i, \ddot{\epsilon}_i, \ddot{\varsigma}_i)^T$ by the time derivative of (13),

$$A_i = \dot{J}_i\dot{q}_i + J_i\ddot{q}_i. \quad (14)$$

Since $\dot{J}_i\dot{q}_i$ was known from (13), the acceleration conversion (14) can be solved with a Jacobian inverse, or a pseudo-inverse, when some DOFs of the manipulator kinematics were excluded,

$$\ddot{q}_i = [J_i^{-1}](A_i - \dot{J}_i\dot{q}_i) \approx [J_i^T J_i]^{-1}[J_i^T](A_i - \dot{J}_i\dot{q}_i). \quad (15)$$

Following [10], a set of fifth order polynomials was defined as:

$$q(t) = D[1\ t\ t^2\ t^3\ t^4\ t^5]^T \quad (16)$$

where the coefficient matrix D can be solved to generate smooth trajectories in ETC between $(q_1, \dot{q}_1, \ddot{q}_1)$ and $(q_2, \dot{q}_2, \ddot{q}_2)$ over the time range $t_1 \leq t \leq t_2$. This standard fifth order polynomial form yielded an analytical solution of the minimum jerk model with boundary conditions represented in the constrained task coordinates ETC [21]. Inspiration for the minimum jerk model came from the core kinematic characteristic of the human motor coordination (i.e., smoothness maximization), the generated ETC trajectories approximate the natural human arm motion as preliminarily tested in [16]. For producing actual control command of the impaired model, the planned motion trajectories needed to be converted into the active arm joint DOF coordinates. For this purpose, the generated ETC trajectories were converted into the Cartesian coordinates by the forward kinematics (see (1) and (2)), and then they were transformed into the active arm joint coordinates by the inverse kinematics as described in [16].

VIII. Validation of the Proposed Model

Diagonal point-to-point human reaching motion setup, with a reduced mobility elbow, as presented in [16], was selected for the desired task. The elbow was constrained by a brace, such that the distance between the center of the shoulder T-joint to the center of the wrist was R = 37.67 cm.

The contact specifications of the hand in the vicinity of each task location can be also geometrically derived using (5)-(7) and are presented in Table I. In order to solve for the six unknown parameters (i.e., each x, y, z coordinate of the base pivot **B** and the moving pivot **P** represented in the fixed frame F), position, velocity, and acceleration design equations at two task locations were solved using PHC. The complex solutions were excluded and the real solution is listed in Table II. The contact specifications at the two task positions in the Cartesian coordinates were then converted into the ETC space via (3) and, (13)-(15). Finally, the joint trajectory was formulated by (16), and the modeled elbow-joint impaired trajectory in Cartesian space was obtained from (1).

Fig. 9 shows the moving frame trajectories of the elbow constrained human hand and the modeled TS chain. For each case, configuration histories of the elbow constrained arm and the TS chain is shown in gray and black, respectively. Note that in the experimental setup, which was simulating reduced elbow mobility, the human elbow was fully locked in place by the brace, the trunk was constrained to a chair, while the shoulder joint SHD shown in Fig. 9 was not fixed. This allowed the subject to use additional shoulder DOFs that were not included in the TS arm model, resulting in the difference between the locations of points B and SHD in Fig. 9. With respect to the reaching paths, the modeled TS chain does not perfectly match the anthropomorphic hand motion profile, however, their geometrical shapes were very similar. Once the shoulder complex is modeled in details and incorporated within the model, it will allow for more robust solutions that simultaneously take into account the patients' existing AROM in the impaired arm and joints and improve the motion profile.

TABLE I
Kinematic Specifications At Two Task Locations of An Elbow-Constrained Arm Performing a Reaching Movement

Specification	Units	Parameters	Initial Location	Final Location
Position	mm	d_x, d_y, d_z	-47.10, 543.7, 51.89	210.0, 493.5, -113.5
	rad	θ, ϕ, ψ	-0.897, -0.853, 0.869	-0.561, -0.612, 1.260
Velocity	mm/s	$\dot{d}_x, \dot{d}_y, \dot{d}_z$	11.88, 0.8770, 1.589	-5.084, 5.984, 16.60
	rad/s	$\dot{\theta}, \dot{\phi}, \dot{\psi}$	0.0314, -0.0326, 0.0696	-0.0297, -0.0280, 0.0257
Acceleration	mm/s²	$\ddot{d}_x, \ddot{d}_y, \ddot{d}_z$	222.4, 24.25, -55.30	-93.72, 41.28, 8.978
	rad/s²	$\ddot{\theta}, \ddot{\phi}, \ddot{\psi}$	-0.562, -2.91, 3.63	-1.35, 0.380, 1.27

TABLE II
Real Solution (All in Mm)

Specification	Parameters	Solution
Fixed pivot at the shoulder T- joint	B = (B_x, B_y, B_z)	142.26, 276.35, -26.568
Moving pivot at the wrist center	$P_1PP = (P_x, P_y, P_z)$	71.402, 456.04, 303.24
Length of the impaired arm model	R	376.71

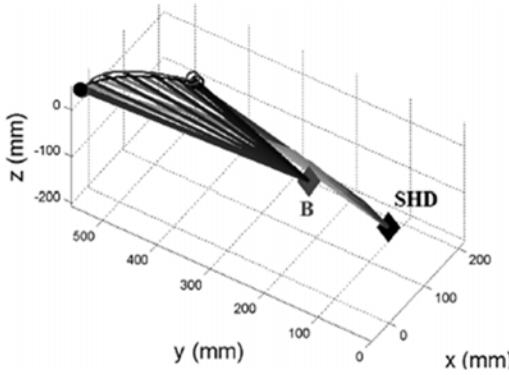

Fig. 9 TS model design solution and path geometry comparison in Cartesian space. B and SHD represent positions of the modeled TS chain and the elbow constrained arm shoulder, respectively

A comparison of the curves geometry and spatiotemporal properties was also conducted. First, each curve was re-parameterized by its arc length, and its Cartesian coordinates were plotted over the normalized arc length (see Fig. 10). The re-parameterization allowed for comparison of the curve geometries without any temporal effects. Next, each x, y, and z-axis components of the two trajectories along the normalized time were compared (see Fig. 11). As shown in those detailed figures, the proposed method closely approximated the geometry and the spatiotemporal aspects of the actual hand path.

Even though the results of the proposed method showed some deviation from the anthropomorphic hand path, it had a unique feature that allowed for the redundant DOF (i.e., the swivel angle γ), which determined the manipulator's configuration during the motion, to be planned separately. From previous experimental observations, it was considered that the human CNS controls the swivel angle in a way to minimize the kinetic energy consumption [14], [19], [21]. Therefore, by implementing an additional trajectory planning

scheme for the swivel angle that minimizes the energy consumption along the determined end-effector trajectory, the elbow impaired model saved the actuating power which may be a crucial advantage for remotely working robotic systems.

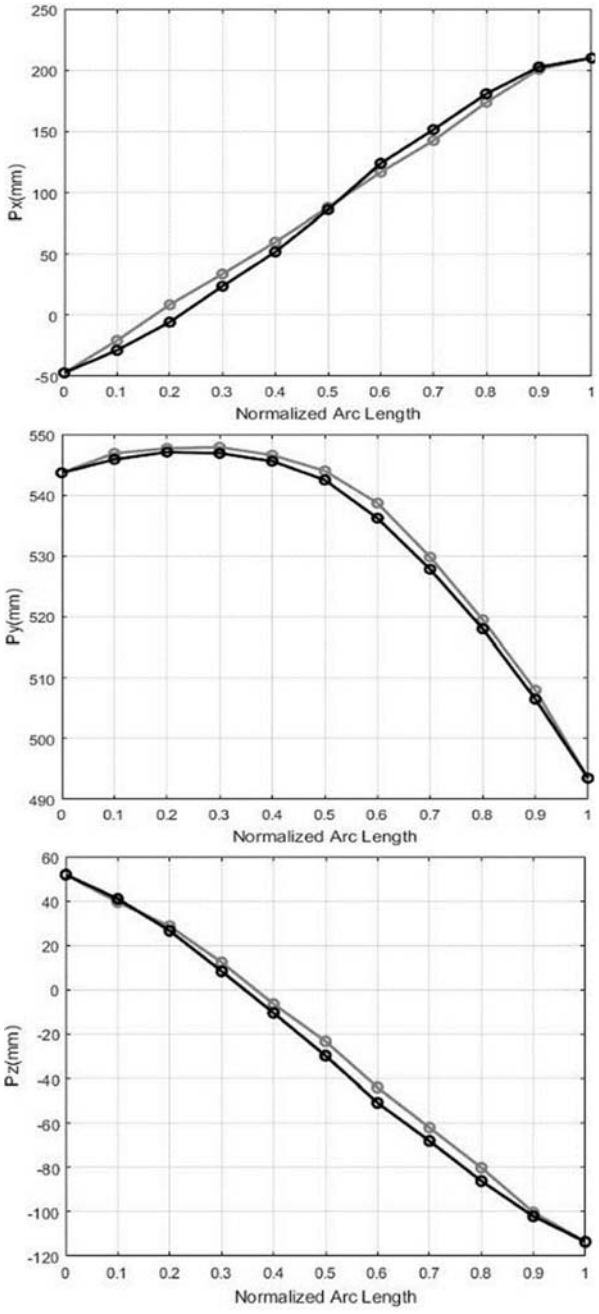

Fig. 10 Trajectory comparison from a geometrical perspective

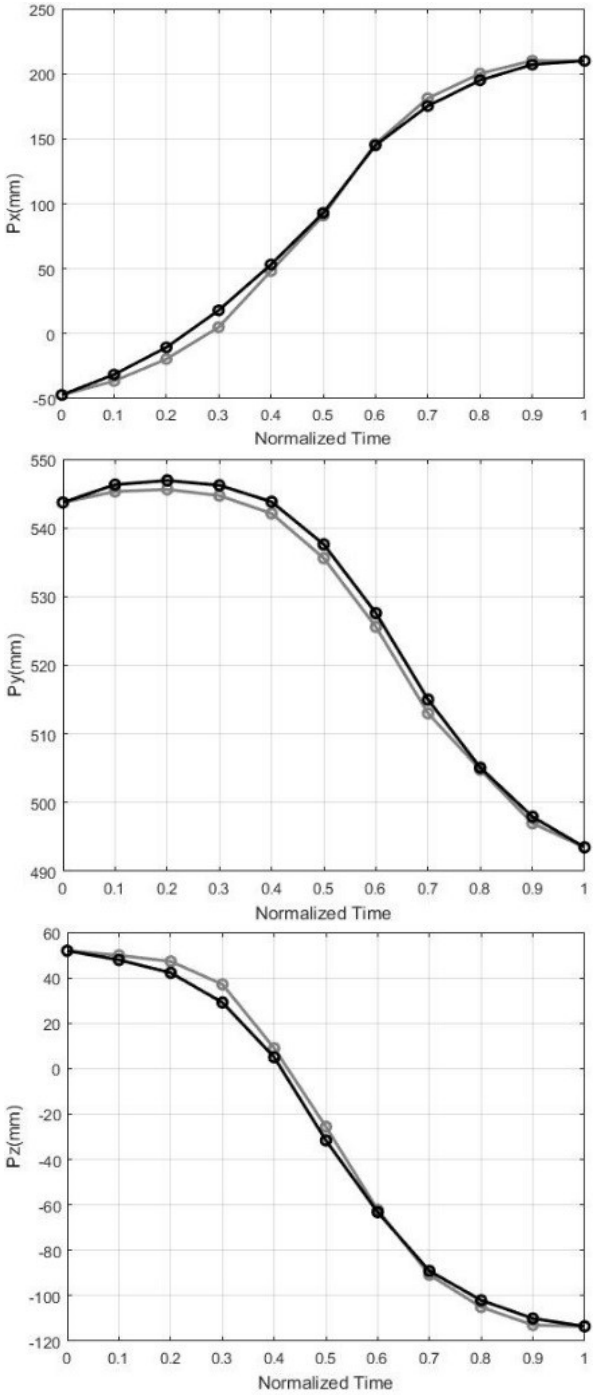

Fig. 11 Trajectory comparison with respect to temporal perspectives

IX. Conclusion

Hand path formulation in a point-to-point reaching motion was a highly redundant mapping problem in mathematics which was resolved by CNS implicitly. In order to incorporate this scheme into the trajectory planning of impaired anthropomorphic arm models, it was proposed that the motion needs to be generated in the constrained task coordinates, which was confirmed by previous experimental studies [14], [19], [20]. As a preliminary study, a spatial TS chain was designed by a recently developed kinematic linkage design

synthesis to approximate the elbow constrained hand motion. In order to specify the design parameters of the TS chain, hand kinematics at the selected task locations was acquired via a motion capture system and the contact geometries at the hand were calculated. These values along with anatomically specific arm data were used to define the position, velocity, and acceleration design equations of the TS chain model, that were solved for the unknown design parameters. Once the model was specified, the kinematic arm skeleton was reconstructed and the reference human hand motion path was modeled via a minimum jerk solution in the human joint space connecting the pre-selected task locations. The model was compared to actual experimental elbow-constrained human hand trajectory using a motion capture system. The proposed model showed a smooth trajectory that closely follows a human-like hand path. Furthermore, it enabled the reformulation of the redundant DOF (i.e., the swivel angle γ) independent of the end-effector trajectory. This feature enables the implementation of other human inspired motor strategies (e.g., minimum kinetic energy principle for posture configuration [14], [19], [21]) to optimize the control performance of anthropomorphic models.

Future work will include a detailed analysis of the approximated model trajectory, compared to the reference human motion profile. In addition, a selection scheme that can determine the optimal design solution according to a measurable performance feature value will be studied to generalize the proposed method. The developed crippled models will be compared to healthy reaching paths and the results will be used in the development of physical training protocols for facilitating the active recruitment of the impaired joint for the successful recovery of patients with limited joint mobility.

ACKNOWLEDGMENTS

The authors gratefully acknowledge the support of the National Science Foundation (NSF), award Id #1404011 and Qatar National Research Fund, National Priorities Research Program sub-award Id # NPRP 7-1685-2-626.

REFERENCES

[1] X. Zhang, P. Braido, S. W. Lee, R. Hefner, and M. Redden, "A Normative Database of Thumb Circumduction In Vivo: Center of Rotation and Range of Motion," *Hum. Factors*, vol. 47, no. 3, pp. 550–561, 2005.

[2] G. Stillfried and P. van der Smagt, "Movement Model of a Human Hand Based on Magnetic Resonance Imaging (MRI)," in *the 1st International Conference on Applied Bionics and Biomechanics (ICABB)*, 2010.

[3] N. Robson and G. S. Soh, "Geometric Design of Eight-Bar Wearable Devices based on Limb Physiological Contact Task," *Mech. Mach. Theory*, vol. 100, pp. 358–367, 2016.

[4] N. Robson and S. Ghosh, "Geometric Design of Planar Mechanisms Based on Virtual Guides for Manipulation," *Robotica*, pp. 1–16, 2015.

[5] N. Robson and G. S. Soh, "Dimensional Synthesis of a Passive Eight-bar Slider Exo-Limb for Grasping Tasks," in *ASME International Design Engineering Technical Conferences*, 2016, p. (Accepted).

[6] N. Robson, "Geometric Design of Mechanical Linkages for Contact Specifications," University of California, Irvine, 2008.

[7] N. Robson, J. M. McCarthy, and I. Tumer, "Exploring New Strategies for Failure Recovery of Crippled Robot Manipulators," in *ASME/IFToMM International Conference on Reconfigurable Mechanisms and Robots (ReMAR)*, 2009, pp. 656–664.

[8] N. Robson and J. M. McCarthy, "Applications of the Geometric Design of Mechanical Linkages with Task Acceleration Specifications," in *ASME International Design Engineering Technical Conferences and Computers and Information in Engineering Conference (IDETC/CIE)*, 2009, pp. 1105–1114.

[9] J. Verschelde, "Algorithm 795: Phcpack: A General-Purpose Solver for Polynomial Systems by Homotopy Continuation," *ACM Trans. Math. Softw.*, vol. 25, no. 2, pp. 251–276, 1999.

[10] J. J. Craig, *Introduction to Robotics: Mechanics and Control*, vol. 3. Upper Saddle River, NJ: Pearson Prentice Hall, 2005.

[11] J. M. McCarthy, *Geometric Design of Linkages*, vol. 11. New York, NY: Springer Science & Business Media, 2006.

[12] J. M. McCarthy, "Mechanism Synthesis Theory and the Design of Robots," in *IEEE International Conference on Robotics and Automation (ICRA)*, 2000, vol. 1, pp. 55–60.

[13] H.-J. Su, C. W. Wampler, and J. M. McCarthy, "Geometric Design of Cylindric PRS Serial Chains," *J. Mech. Des.*, vol. 126, no. 2, pp. 269–277, 2004.

[14] H. Moon, N. P. Robson, R. Langari, and J. J. Buchanan, "Experimental Observations on the Central Nervous System's Governing Strategies on the Arm Reaching with Reduced Mobility," in *ASME International Mechanical Engineering Congress and Exposition (IMECE)*, 2012, pp. 483–492.

[15] X. Wang, "Three-Dimensional Kinematic Analysis of Influence of Hand Orientation and Joint Limits on the Control of Arm Postures and Movements," *Biol. Cybern.*, vol. 80, no. 6, pp. 449–463, 1999.

[16] H. Moon, N. P. Robson, and R. Langari, "Approximating Constrained Hand Paths via Kinematic Synthesis with Contact Specifications," in *Advances in Robot Kinematics*, New York, NY: Springer Science & Business Media, 2014, pp. 375–384.

[17] N. Robson and A. Tolety, "Geometric Design of Spherical Serial Chains with Curvature Constraints in the Environment," in *ASME International Design Engineering Technical Conferences and Computers and Information in Engineering Conference (IDETC/CIE)*, 2011, pp. 289–295.

[18] N. Robson and J. M. McCarthy, "Synthesis of a Spatial SS Serial Chain for a Prescribed Acceleration Task," in *the 12th World Congress on Mechanism and Machine Science (IFToMM)*, 2007.

[19] H. Moon, N. P. Robson, R. Langari, and J. J. Buchanan, "Experimental Observations on the Human Arm Motion Planning Under an Elbow Joint Constraint," in *International Conference of the IEEE Engineering in Medicine and Biology Society (EMBS)*, 2012, pp. 3870–3873.

[20] H. Moon, N. Hoang, N. P. Robson, and R. Langari, "Human Arm Motion Planning Against a Joint Constraint," in *the 4th IEEE RAS & EMBS International Conference on Biomedical Robotics and Biomechatronics (BioRob)*, 2012, pp. 401–406.

[21] H. Moon, N. P. Robson, R. Langari, and S. Shin, "An Experimental Study on Redundancy Resolution Scheme of Postural Configuration in Human Arm Reaching with an Elbow Joint Kinematic Constraint," in *the 2nd Middle East Conference on Biomedical Engineering (MECBE)*, 2014, pp. 257–260.